Photochromic Organic–Inorganic Nanocomposites as Holographic Storage Media

P. Judeinstein,* P. W. Oliveira, H. Krug and H. Schmidt
Institut für Neue Materialen, Universität des Saarlandes, Geb. 43, D-66123 Saarbrücken, Germany

This paper describes the properties of some new organic–inorganic photochromic layers. They are based on a hybrid organic–inorganic matrix in which tungsten heteropolyoxometallates ($SiW_{12}O_{40}^{4-}$, $PW_{12}O_{40}^{3-}$) are entrapped in a network obtained from the reaction of 3-glycidoxy-propyltrimethoxysilane. The high homogeneity of these materials on the nanoscale leads to transparent monoliths and layers of controlled thicknesses up to 40 μm. The optical properties of the blend are emphasised and the construction of amplitude gratings in the materials by two-wave-mixing experiments is described. The results of the optical experiments and the comparison with the theoretical background are used as a model for photochromic holographic storage processes.

KEYWORDS nanocomposites; sol–gel; heteropolymetallates; photochromics; holographic data storage; amplitude grating; two-wave-mixing recording

I. INTRODUCTION

New and future computer technologies should be able to manage and process extensive sets of data. Optical holographic recordings can be considered as an answer to such inquiries if real-time optical storage media capable of efficient, reversible and fast recording are used.[1,2] Nanotechnologies are looking to reach such goals and the photochromic properties of some materials are an interesting alternative to reach them.[3] Then, in order to improve the data density, materials with ultra-high-resolution capabilities have to be used. Photochromically sensitive units as small as possible and with the highest contrast variation between bleached and coloured states should be entrapped in a polymeric or glassy matrix.[4] Such high-tech substances can be described as nanocomposites.[5] They should combine and synergise the properties of a well-suited solid matrix and well-suited photosensitive molecules or clusters.[6]

The sol–gel process is an interesting route to prepare nanocomposites.[7] This low-temperature process allows the synthesis of materials which cannot be prepared by conventional methods. Moreover, the control of the viscosity of the mother solution is a key to preparing films of variable thicknesses on different surfaces as well as monoliths of various shapes.[8]

However, well-suited materials are not enough; optimisation of the data storage process requires also detailed knowledge of the grating formation mechanism. The determination of the parameters involved in the diffraction efficiency is the key to the enhancement of the properties. Both the film characteristics (photochromic cluster concentration, film thickness, etc.) and the write–read apparatus set-up (laser wavelength, irradiation power and time, etc.) are involved in the grating

* Current address: Laboratoire de Chimie Structurale Organique (URA CNRS 1384), Université Paris Sud, Bât. 410, F 91405 Orsay, France.

performance. Indeed, one of the main factors determining the feasibility of a holographic storage system concerns the possibility to use a smaller and cheaper laser for writing and read-out.

This paper presents the behaviour of some new organic–inorganic nanocomposites to be used for optical data storage. Their synthesis and chemical characterisation are presented. They are important for their photochromic properties and this paper emphasises their use as holographic storage media.

The active photochromic molecules are tungsten heteropolyoxometallates, $M'W_nO_{3n}^{x}{}_{m}$ (or POMs).[9] These molecules have a very high electron density and the presence of many highly oxidised metallic centres makes them good candidates for redox-based applications[10] (catalysts, analytical reagents, materials for photochemistry and electrochromism, etc.). A reduction reaction can switch these molecules from colourless to dark blue upon UV irradiation, while bleaching corresponding to an oxidation reaction occurs upon O_2 contact.[11]

Reactive organosilanes ($(XO)_3SiR$) are used as the basic reagents to get functionalised networks. 3-Glycidoxy-propyltrimethoxysilane (GPTS) has already been found suitable to dissolve high quantities of POMs and then react to form a transparent matrix.

In Section 2 the synthesis and structure of these new materials will be described to highlight the flexibility of the sol–gel synthesis pathway and the possibilities to tune the properties of the nanocomposite films (thickness, optical properties). In Section 3 the properties that make them suitable as media for holographic data storage are discussed. Real-time measurements are described that allow *in situ* probing of the grating formation and characteristics. The experimental results are compared with the theoretical background for amplitude grating construction in films.

2. NANOCOMPOSITES: SYNTHESIS AND CHARACTERISATION

2.1. Experimental

All chemical reagents were commercially available and were used as purchased: 3-glycidoxy-propyltrimethoxysilane (GPTS), silicotungstic and phosphotungstic acids (respectively $H_4SiW_{12}O_{40}$, abbreviated as SiW_{12}, and $H_3PW_{12}O_{40}$, abbreviated as PW_{12}). Deionised water was used in all experiments. Two series of compounds have been synthesised with a constant hydrolysis ratio h ($h = [H_2O]/[GPTS] = 2.5$) and POM ratios p between 0.05 and 0.8 ($p = [W]/[GPTS]$). The following notation will be used: $[X]_p$, where X is the central heteroatom of the POM (Si or P).

NMR measurements have been performed with AC 200 and AM 200 Bruker spectrometers, for liquid and solid state experiments respectively, following standard procedures (^1H–^nX decoupling for liquid measurements, cross-polarisation and magic angle spinning (CP-MAS) for solid state measurements ($^nX \equiv {}^{13}C$, ^{29}Si)).

Photochromic reactions have been performed with 750 W xenon lamp illumination. Optical absorption measurements were made with an Omega 10 spectrometer (Bruins Instruments) with 2 nm optical resolution.

2.2. Gel Preparation

The synthesis of the $[Si]_{0.8}$ material is described.

A mixture of 2.36 g of GPTS (0.01 mol) and 0.9 g of water (0.05 mol) was vigorously stirred. Then 1.98 g of SiW_{12} (6.6×10^{-4} mol) was slowly added and a highly exothermic reaction occurred. The mixture was stirred for 5 min and the viscosity of the reaction bath increased rapidly. Dip coating or spin coating was used to make films on different substrates (glass, metal, plastic, etc.). Depending on the viscosity and the deposition conditions, films from about 0.5 to 50 μm thick have been obtained. The gelation time is about 5 h and casting of the solution in a Teflon mould leads to transparent monoliths. Materials were dried for 48 h at 90 °C before further studies. The gel time is quite sensitive to the POM nature and concentration, ranging from 4 h for $[Si]_{0.8}$ to more than 100 h for $[P]_{0.05}$ blends.

2.3. Gel Characterisation

2.3.1. ^{29}Si NMR

Liquid state ^{29}Si NMR experiments have been performed to follow the chemical evolution of the system. Immediately after mixing of the starting reagents and for the whole range of POM concentrations, the spectrum presents three peaks around −48, −57 and −65 ppm, characteristic of T^1, T^2 and T^3 units respectively.[12] The absence of

T^0 species and the low ratio of T^1 units immediately after mixing of the reactants highlight the fast condensation rate of silica species. The high-field signal is broad, evidencing the size distribution and short relaxation time of T^3 units. Fig. 1 presents the CP-MAS ^{29}Si NMR spectra of $[Si]_{0.2}$ and $[Si]_{0.8}$ materials. The spectrum of the blend containing the lower SiW_{12} ratio presents two peaks centred around -58 and -65 ppm (T^2 and T^3 units), while the material containing the higher concentration of POM yields only a broad peak around -67 ppm, characteristic of T^3 species, and a weak peak around -85 ppm, characteristic of the central silicon atom of POM Keggin species. These experiments illustrate the fast kinetics of the hydrolysis–condensation reactions in comparison with the gelation process. In the final material the predominance of the fully condensed T^3 species indicates that compact silica clusters are the inorganic framework of these materials. The influence of the acidic ratio (POM concentration) on the silica condensation state is observed.

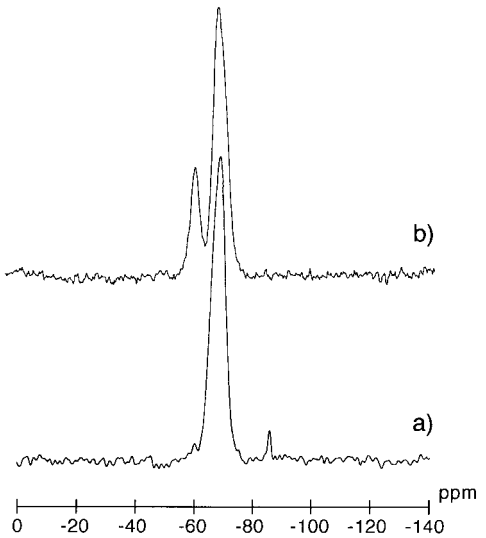

Fig. 1. CP MAS ^{29}Si NMR spectra of (b) $[Si]_{0.2}$ and (a) $[Si]_{0.8}$ composites

2.3.2. ^{13}C NMR

The ^{13}C NMR spectrum of the $[Si]_{0.8}$ blend diluted in acetone-d_6 after mixing of the reactants has been recorded. Many changes are observed in comparison with the spectrum of pure GPTS. First of all, the disappearance of the 50.5 ppm signal and the appearance of a signal at 49.7 ppm confirm the rapid hydrolysis of the silicon atom and the subsequent formation of methanol as a by-product. Furthermore, the relative intensity of most of the other peaks decreases strongly and many new peaks appear, evidencing the reactivity of the epoxy group. Two different reactions could occur after the breaking of the epoxy bond in such a strongly acidic medium, as presented in Fig. 2: the formation of a diol or the development of a polyether

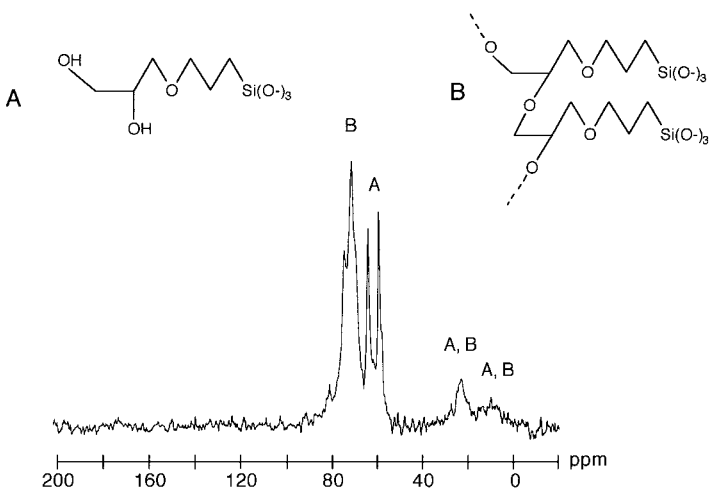

Fig. 2. CP MAS ^{13}C NMR spectrum of $[Si]_{0.8}$ composite. Tentative attribution of the peaks is made according to two reaction schemes: A, diol formation; B, polycondensation reaction

network.[13] The CP-MAS spectrum of the solid material is also presented in Fig. 2. The broad peaks around 10 and 23 ppm are characteristics of the alkyl spacer (—O—CH_2(CH_2)$_2$—Si) bonded to silica clusters with a large size distribution and reduced mobility. The formation of the diol species (CH_2—CHOHCH_2OH) is evidenced by sharp peaks at 59 and 69 ppm. The broad peaks around 71 and 74 ppm evidence the formation of polyethylene chains (—OCH(CH_2O—)$_2$) resulting from the condensation of epoxy groups. The relatively strong intensity of this set of peaks indicates that under the experimental conditions the formation of polymers is favoured after the epoxy breaking. No major changes have been observed when lower POM concentrations are used down to $[X]_{0.05}$. This suggests that in both cases a high yield of polymerisation has been reached and POM species behave as a good catalyst to improve the epoxide addition reaction in comparison with the diol formation.[14]

2.3.3. IR

Infrared spectra present broad bands characteristic of poly(ethylene oxide) ($\nu_{C\ O\ C}$, 1170 cm^{-1}; $\nu_{C\ H}$, 2940–2880 cm^{-1}) and silica clusters ($\nu_{Si\ O\ Si}$, 1070 cm^{-1}). Before further drying, hydration of the film is evidenced by two bands around 3500 and 1600 cm^{-1}. Intense peaks characteristic of POM species are well defined, e.g. for $[Si]_{0.8}$: 1016 cm^{-1} ($\nu_{asSi\ O}$), 969 cm^{-1} ($\nu_{asW=O}$), 920 cm^{-1} ($\nu_{asSi\ O/W\ O\ W}$), 886 cm^{-1} $\nu_{asW\ O\ W}$), 795 cm^{-1} ($\nu_{asW\ O\ W}$). The band wave numbers are rather similar to those observed for POMs in solution in common solvents and the small shifts observed therein reflect the anion–cation and anion–solvent interactions.[15]

2.3.4. UV–visible

POM species entrapped in the hybrid matrices could be reduced under UV light. Before reduction the films show no significant absorption between 360 and 1800 nm. Fig. 3 presents the optical absorption spectra of the reduced thin films $[Si]_{0.8}$ and $[P]_{0.8}$. These spectra show some defined bands, with maxima around 500, 745 and 1270 nm for PW_{12}-doped materials and around 490, 718 and 1108 nm for SiW_{12}-doped materials. They are characteristic of reduced Keggin molecular species, with d–d bands in the visible range and charge transfer intervalence transitions W^{5+}–W^{6+} in the near IR.[16]

2.3.5. EPR

EPR is an efficient and sensitive spectroscopy to characterise reduced polymetallates. Samples have been reduced under a low-power UV light before investigation. Measurements have been performed at 90 K. The $[P]_x$ materials present an isotropic signal centred at $g = 1.815$, while the $[Si]_x$ materials show a rather orthorhombic signal ($g_x = 1.857$, $g_y = 1.825$, $g_z = 1.786$). These values are in perfect agreement with values reported in the literature.[17] The orthorhombic symmetry of $H_4SiW_{12}O_{40}$ is explained by electron localisation at a temperature around 90 K.

The structural investigations of these materials demonstrate their nanocomposite characteristics. Small tungsten oxide clusters (POMs) are entrapped inside a hybrid organic–inorganic matrix. The POM clusters are homogeneously distributed inside the materials and their photochromic properties as individual molecules remain even in the most heavily doped materials. Strong blue coloration is obtained under UV light. This is associated with intramolecular electron transfer and could be described as a polaronic electron-hopping process. Then bleaching could occur when the material is in contact with ambient air or O_2. Bleaching times from 2 to 24 h are measured depending on the reduction ratio. In the absence of air the colour remains and no bleaching has been observed even after a couple of months if the

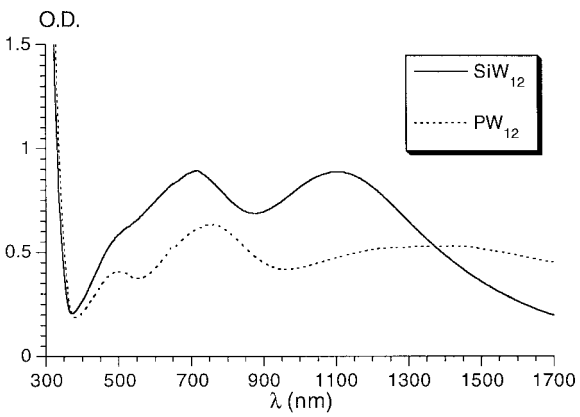

Fig. 3. UV visible spectra of $[Si]_{0.8}$ and $[P]_{0.8}$ materials

materials are covered by a protective layer of sol–gel silica or organic varnish.

The matrix is made of organic and inorganic parts strongly connected through stable carbon–silicon bonds. The grafting of the two phases leads to a strong stability of these materials against heating (up to 150 °C) or humid atmosphere in comparison with materials in which the organic and inorganic parts are only partially connected.[7b,18]

These materials are synthesised under strong acid catalysis obtained by the dissolution of a large amount of POM. Then silicon alkoxide and epoxy groups evolve in parallel with kinetics of comparable range, leading to silica clusters and polyether chains respectively. The rigid backbone of these materials comes from the intimate interpenetration of these two phases. The high solubility of POM molecules inside poly(ethylene oxide) chains has been previously described as coming from the oxygen lone pairs. This enables the nanoscale dispersion of the components—silica clusters, polyether chains and POM species—leading to a transparent material.

For further optical investigations, films approximately 20 μm thick were deposited on glass or quartz glass slides by the dip-coating method and dried for 24 h at 110 °C.

3. NANOCOMPOSITES: GRATING FORMATION

3.I. Experimental Set-ups

The experimental set-up used for real-time write–read holographic experiments is shown schematically in Fig. 4. Optical absorption gratings in thin films are obtained by two-wave-mixing techniques. Laser writing is performed with an Ar^+ laser at 351 nm. The light is split into two beams of 1 mm diameter and up to 20 mW power each. The two beams intersect with an angle of about 2° on the sample and create an interference pattern with standard periodicities in the range 10–15 μm. For further investigations, interference patterns with periodicities from 2.5 to 30 μm could be achieved. The incident waves are symmetric, so the grating fringes are parallel to the material surface and the shape of every fringe is the same. The efficiency is determined in transmission mode with a reading helium–neon laser of low intensity ($\lambda = 633$ nm, $I_i \approx 5$ mW). Then diffraction peaks are observed for Bragg angles. The optical system is set up to measure the evolution of the first-order diffraction peak with time, $I_{\pm1}(t)$,[19] and the efficiency is defined as $\eta_{\pm1}(t) = I_{\pm1}(t)/I_i$.

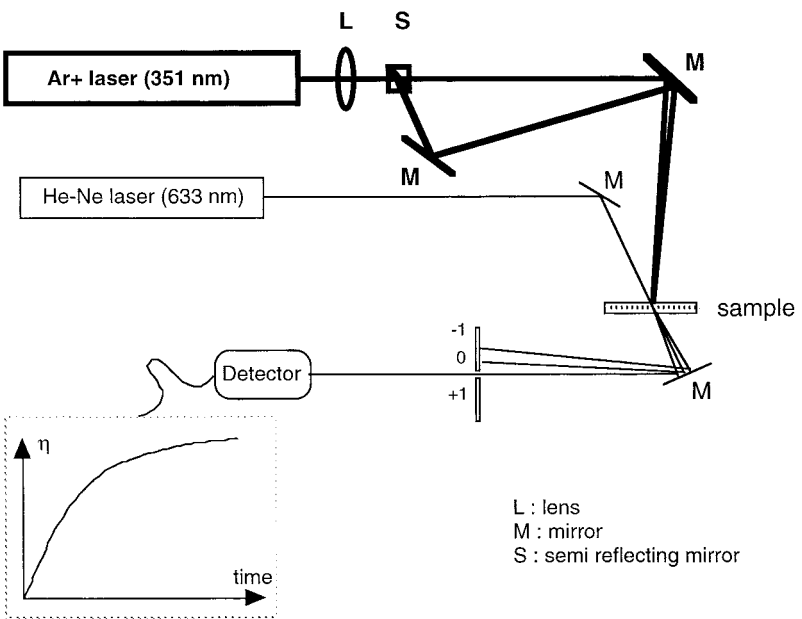

Fig. 4. Optical holography set up

The reading and writing beams are quite parallel and the reading beam can be distinguished in the detector photocell by a polariser and a filter. The measurements are made near the diffraction pattern centre region, where the approximation of a planar grating is quite correct, which is required to compare the experiments with the theoretical background.[20]

In another experiment the interference pattern of the incident UV light and the grating absorption profile have been determined with a videocamera-based charge-coupled device.[21] The sample is illuminated with white light and the absorption profile is measured in transmission mode with a camera (Silicon Camera model LBA-100) equipped with microscope lenses. The data are analysed with a Spiricon laser beam analyser connected to a computer for digitalisation. A spatial resolution of 1 μm^2 has been achieved for these measurements.

Another experimental set-up has been used for monitoring in real time the measurement of the absorption of the photochromic layer under different incident laser powers. The light of the writing Ar^+ laser is focused as a 1 cm^2 beam. The reading He–Ne laser is aligned in the same direction and the detector is placed after a filter and a polariser.

For all these experiments the power of the writing Ar^+ laser has been checked with a power meter. The thickness of the films is kept constant at 20 μm for all samples. Then the difference between thick and thin gratings is only related to the variation in the Q-factor, $Q = 4\pi\lambda d/\Lambda^2 n$, where λ is the wavelength, d is the thickness of the film, Λ is the grating periodicity and n is the refractive index of the layer. The grating is considered as thick for $Q \gg 1$ and as thin for $Q \ll 1$ (*vide infra*).[22,23]

3.2. Construction of an Absorption Grating

Fig. 5 presents the microphotograph of an absorption grating produced by two-wave mixing. Alternate coloured and transparent stripes with 10 μm periodicity are observed. They result from the photochromic reaction of POM species entrapped in the matrix which are irradiated by modulated UV light. The efficiency $\eta_{\pm 1}$ has been measured in real time during writing irradiation. The influence of parameters such as exposure time, grating thickness (resolution) and POM concentration has been checked. A maximum value of $\eta_{\pm 1} = 6.1$ has been measured for a thin grating ($\Lambda = 10$ μm) with a POM ratio of 0.8 and an exposure time of 5 min with two 20 mW beams. Lower efficiencies have been measured for lower POM ratios. We noticed also that shorter or longer exposure times led to lower efficiencies. In regard to these preliminary results, the process of amplitude grating formation inside photochromic materials should be analysed. This analysis is developed in the following subsections in order to present the tools which are necessary to forecast the properties of such gratings and optimise their applications.

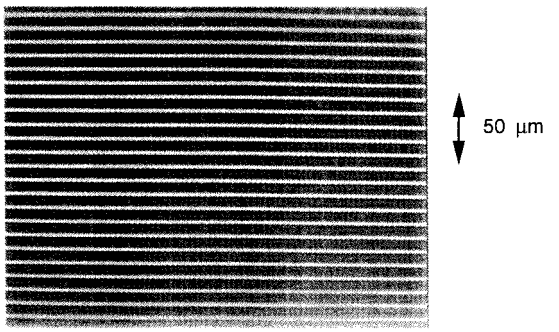

Fig. 5. Microphotograph of an absorption grating

3.2.1. Photochromic process

In essence, the grating formation inside the material is related to the photochromic process of the POM species. The strong absorption of the UV light and the resulting POM photoreduction are well documented.[11] The simultaneous oxidation of a neighbouring molecule is implicated. In the presence of traces of alcohol the formation of carbonyl has been observed. The following mechanism can be suggested:

$$\mathrm{POM}^{n} \xrightarrow{h\nu} \mathrm{POM}^{*n}$$

$$\mathrm{POM}^{*n} \xrightarrow{k_1} \mathrm{POM}^{n}$$

$$\mathrm{POM}^{*n} + \mathrm{RCH_2OH} \rightarrow \mathrm{POM}^{(n+1)} + \mathrm{R\dot{C}HOH} + \mathrm{H}^+ \quad (k_{\mathrm{Q}})$$

$$\mathrm{POM}^{n} + \mathrm{R\dot{C}HOH} \rightarrow \mathrm{POM}^{(n+1)} + \mathrm{RCHO} + \mathrm{H}^+ \quad (k_{\mathrm{R}})$$

$$\mathrm{POM}^{(n+1)} + \mathrm{R\dot{C}HOH} \rightarrow \mathrm{POM}^{(n+2)} + \mathrm{RCHO} + \mathrm{H}^+$$

$$\mathrm{POM}^{(n+2)} + \mathrm{POM}^{n\ 1} \rightarrow 2\mathrm{POM}^{(n+1)}$$

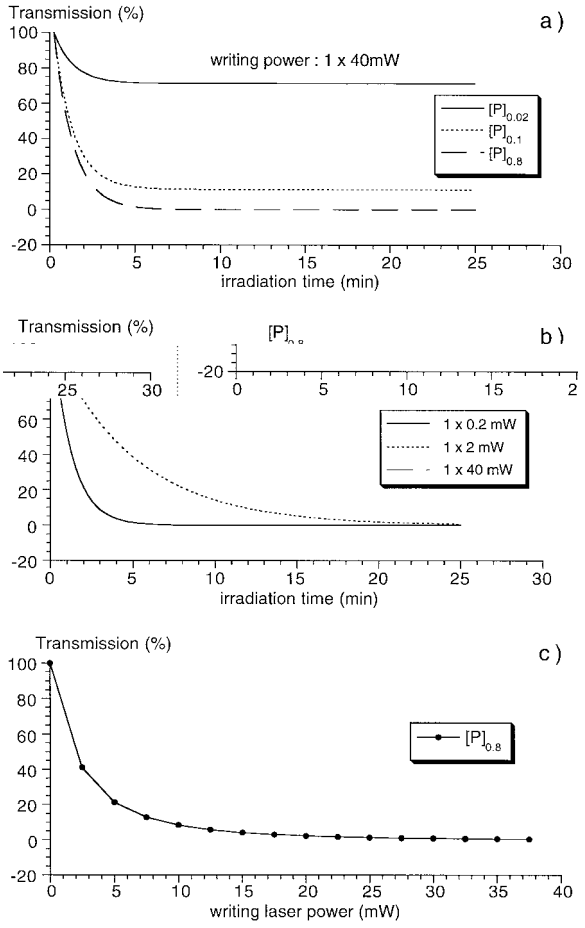

Fig. 6. Photoreduction process. Real time evolution of optical transmission of layers: (a) variation in optical density (OD) with POM concentration; (b) variation in OD with incident laser power; (c) relation between OD and laser power after 5 min irradiation

POM^n is the completely oxidized form of the polymetallate, while $POM^{(n+1)}$ is a dark coloured, mixed valence compound. Theoretically, one photon is necessary to reduce two molecules, but obviously the yield is much lower than unity as a result of de-excitation backward reactions (k_{-1}). These backward reactions are mainly due to the interaction with the matrix, light absorption, etc.

Then an accurate analysis of the photochromic behaviour of these materials under experimental conditions is the first step towards analysing further the grating formation and properties. Fig. 6(a) presents the variation in the optical transmission of films measured in real time during UV irradiation (40 mW) and for different POM concentrations. During the first 5 min the transmission decreases, corresponding to the development of the photochromic reaction. Thereafter the saturation of the coloration is observed, corresponding to the completion of the reaction. At this point all POM molecules can be considered as reduced and the classical Beer–Lambert relationship is confirmed ($\varepsilon_{632} = 0.75$ cm^{-1} g^{-1} l). Fig. 6(b) presents the evolution of the transmission for the film $[P]_{0.8}$ with different laser intensities. A strong dependence of the time to complete the photoreduction is observed. This time ranges from less than 5 min for 50 mW power, to 20 min for 10 mW and a few hours for 1 mW. After completion of the reaction the final coloration level is only dependent on the POM concentration. Fig. 6(c) presents the variation in the film optical transmission with the writing beam intensity after 5 min of light exposure. A strong decrease in the absorption is observed for illumination times up to 15 min, where it reaches a value of 5%. Twice this delay is required to complete the photoreduction to less than 1% of the light transmission.

3.2.2. *Grating formation*

The writing modulation of the light is produced as an interference pattern obtained by two-wave mixing. The equation describing the spatial modulation of the light is

$$I(x, y) = I_0 \exp[-(x^2 + y^2)/r_0^2][\cos(kx) + A] \quad 1$$

where (x, y) are the co-ordinates of the point with respect to the centre of the pattern, $k = 2\pi/d$, $d = \lambda/2 \sin(\alpha/2)$, λ is the wavelength of the light, α is the angle between the two beams, r_0 is the radius of the laser beams and A takes into account the ratio between the intensities of the two laser beams. Then the interference pattern is a Gaussian profile modulated by a sinusoidal variation and can be considered as a pure sinusoidal profile near the centre of the spot ($x, y \approx 0$, planar surface approximation).

Fig. 7 presents the experimental transmission profile obtained by densitometry very near the beam centre. This profile is well described by Eqn. 1 with $(x^2 + y^2)/r_0^2 = 1$ (planar wave approximation), $I_0 = 37$ mW, $A = 2/37$ and $k =$

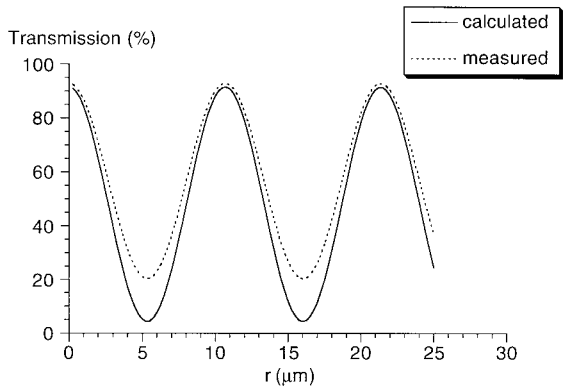

Fig. 7. Absorption profile of layer (densitometry) compared with theoretical curve

1/12 μm [1]. A semiempirical approach to calculate such a grating profile has been developed from the knowledge of both the light profile and the dependence of the film transmission on the illumination (as presented in Fig. 6(c)). This theoretical shape obtained by numerical resolution is close to the experimental result (Fig. 7, full line). The small discrepancy between the theoretical calculation and the experimental result can be explained by destructive interferences created between the light scattered by the substrate or material defects and the interference writing pattern and also by the small power difference between the two beams. These errors are very small, so the grating can be described by a spatially modulated transmission function. Moreover, the optical properties vary slowly in spatial dimensions comparable with the wavelength, so a plane wave approximation is possible.

3.3. Efficiency of Absorption Grating

A more universal way to characterise a grating is to measure the so-called efficiency $\eta_{\pm 1}$, which is defined by the ratio $I_{\pm 1}/I_0$, where I_0 is the intensity of the reading beam and $I_{\pm 1}$ is the intensity of the first Bragg diffraction peak. A more reliable way to measure its value is to use an experimental set-up such as that presented in Fig. 4. To go further in the theoretical determination of the efficiency, the thickness factor of the grating, Q, has to be defined:

$$Q = 4\pi\lambda d/\Lambda^2 n \qquad 2$$

where λ is the writing wavelength, d is the thickness of the film, Λ is the grating periodicity and n is the refractive index of the photochromic material. The grating is considered as thick if $Q \gg 1$, while it is considered as thin if $Q \ll 1$.

For a thick grating, amplitude grating theory states that the diffraction efficiency is

$$\eta_{\pm 1} = I_{\pm 1}/I_{\mathrm{i}} = \exp(-kd/\cos\alpha)\sinh^2(\Delta k d/4\cos\alpha) \qquad 3$$

where k is the absorption coefficient at 632 nm, Δk is the maximal absorption coefficient variation between dark and pale zones and α is the angle between the writing and the reading angle. A maximum theoretical efficiency of 3.7% can be achieved.

When a thin grating is considered, the real refractive index can be considered as constant and the imaginary refractive index changes with the absorption as $\Delta\tilde{n} = \Delta k/4\pi$. The amplitudes of the diffraction waves are given by

$$A_m = (A_{\mathrm{i}}/\Lambda)\int_0^{\Lambda} \exp\{\mathrm{i}[\Phi\cos(2\pi x/\Lambda)] + m2\pi x/\Lambda\}\,\mathrm{d}x \qquad 4$$

where Φ is the phase shift, defined as $\Phi = 2\pi\Delta\tilde{n}d/\Lambda$. The diffraction efficiency is $\eta_m = (A_m/A_{\mathrm{i}})^2$, where A_{i} is the amplitude of the incident light.

The diffraction efficiency of the first-order diffraction is given by the Bessel function as

$$\eta_{\pm 1} = |j_{\mathrm{i}}(\Phi)| \qquad 5$$

The maximum of the diffraction efficiency of a thin amplitude grating is obtained for 100% modulation of the absorption and a value of 6.25% is then expected. A maximum value of 6.1% was measured in our thin films, expressing the high contrast between dark and pale zones of the printed grating pattern. Evidently, these measurements are also in good agreement with the densitometry results.

3.4. Properties of Gratings

3.4.1. *Influence of irradiation time*

Fig. 8 presents the real-time evolution of the efficiency $\eta_{\pm 1}$ for both thin and thick gratings,

corresponding to interference pattern periodicities Λ of 2.5 and 30 μm respectively. The $\eta_{\pm1}$ evolution curve presents the same behaviour for the different grating categories. During the initial period a rapid increase in the grating efficiency is observed. The maximum value of $\eta_{\pm1}$ is measured after an irradiation time of about 5 min ($\eta_{\pm1} = 5.5$ and 2.2 for thin and thick gratings respectively). For longer illumination times an exponential-like decrease in the efficiency is observed down to a very low value: $\eta_{\pm1} = 1.5$ and 0.2 for thin and thick gratings respectively after UV irradiation of 25 min. This behaviour disagrees with the usual trends measured in volume phase holograms, where the saturation of the efficiency is observed after completion of the reactions.[25]

These differences can be explained by the mechanism of grating formation and the variation in film absorption with irradiation time (Fig. 6(b)). For short irradiation time the contrast Δk between high- and low-absorption zones increases quickly, leading to the rapid and efficient construction of the grating. The saturation of the coloration in the dark zones is obtained after 5 min; during this delay the optical absorption of the pale zones is slightly affected and more than 98% of the transmission remains after 5 min irradiation. This time corresponds also to the irradiation time to get the highest contrast of the grating and thus a better efficiency. For longer irradiation times the backward reaction strongly decreases the absorption of the less coloured stripes, corresponding to a decrease in the grating contrast and the destruction of the interference pattern. This is in agreement with the measured decrease in the efficiency. An empirical calculation of the variation in the diffraction efficiency can be performed from the experimental variation in the film transmission with time and different writing powers (as presented in Fig. 6(b)). For each irradiation time the first step of the calculation is the determination of the grating profile (Eqn. 2). Then the efficiency is calculated by Eqn. 3 or 4. The results are presented in Fig. 8 for both thin and thick gratings in $[P]_{0.8}$ materials. Then the analytical variation in the efficiency with time has been computed and plotted in Fig. 8 for both thick and thin gratings in $[P]_{0.8}$ materials. The shape of the empirical curves is in good agreement with the experimental trends, showing a two-stage grating behaviour: the construction of the grating for shorter times and its destruction for longer irradiation times. The second stage of the curve is related to the quality of the writing interference pattern. For an ideal interference pattern the out-of-phase intensity is zeroed and a longer writing period should have no destructive effect.

3.4.2. *Influence of POM concentration*

Fig. 9 presents the variation in the first-order diffraction efficiency $\eta_{\pm1}$ with the POM content $[P]_n$, measured after 5 min UV irradiation in thin gratings. This irradiation time corresponds to the maximum of the diffraction efficiency. These measurements evidence the strong variation in the grating efficiency with the POM concentration. For lower POM concentrations the contrast Δk is low, even when the illumination time is infinite (Fig. 6(a)), leading to a low value of the diffraction

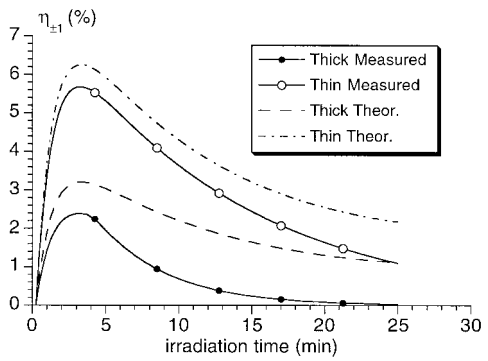

Fig. 8. Real time evolution of diffraction efficiency for both thick and thin gratings, experimental and theoretical curves (in phase and out of phase intensities of 37 and 2 mW respectively)

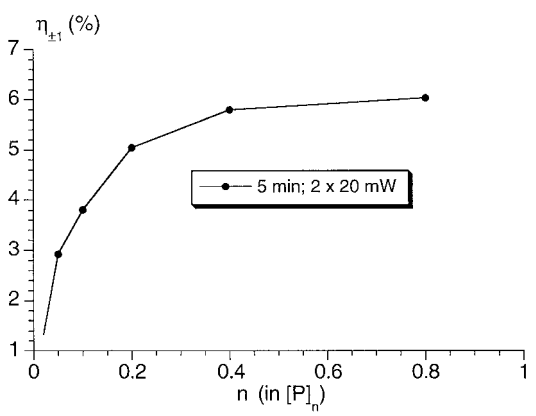

Fig. 9. Diffraction efficiency: variation with POM content

efficiency. Higher efficiency values can be reached when the contrast Δk increases, ie the POM concentration increases. For POM concentrations higher than 0.4 the value of $\eta_{\pm 1}$ reaches a maximum of 6%. This value is close to the theoretical maximum value (6.25%). From the knowledge of the variation in the optical absorption with the POM concentration an empirical value of the grating efficiency can be calculated. These values are plotted in Fig. 9 and are in good agreement with the experimental values.

4. CONCLUSIONS

The possibility of mixing together organic and inorganic components to get hybrid materials is a key to producing new functional materials with improved properties. Efficient photochromic materials have been described. Their behaviour for amplitude grating recording demonstrates their potentialities as holographic media. The flexibility of the sol–gel process facilitates the tuning of the layer properties: thickness, POM content, absorption properties, etc. Very high concentrations of POMs can be achieved inside the materials, leading to strong photochromic contrasts. Then gratings with almost theoretical maximum efficiencies have been printed inside the layers. Their properties have been compared with the theoretical background with good agreement. In particular, the very good optical properties of the layers enable these good experimental results. This comes from the mixing of the different components of the layers at the molecular level and the high compatibility between the different phases.

The detailed study of the properties of the absorption gratings evidences the interesting behaviour of these organic–inorganic hybrid materials. A high efficiency of the grating is achieved for moderate POM content ($[P]_{0.4}$) and short irradiation time (5 min). No improvement in the grating is observed for higher POM ratios, while a strong degradation is observed for longer writing times. This last effect is related to the quality of the writing pattern, ie the ratio of in-phase and out-of-phase intensities. After printing, the grating remains without degradation for a long time if the layer is protected from the air by a protective film. This can be explained by the very low diffusion coefficient D_e of the POM species inside the dried matrices, as measured by forced Rayleigh scattering in similar materials ($D_e \ll 10^{-12}$ cm^2 s^{-1}).[26] Moreover, these materials can be considered as permanent or temporary storage media, depending on the atmosphere they are in. Erasing is achieved by contact with the air for a few days or quicker by an O_2 gas flow, and probably better control of the bleaching kinetics could be achieved by adding an oxidant inside the layer.

Finally, this study emphasizes the possibility to forecast easily the properties of materials for optical storage. Only a very limited set of data concerning their photochromic properties is necessary: transmission as a function of time, irradiation power and photochromic dye. Then semiempirical calculations enable us to determine the grating efficiency for different writing conditions (writing light profile, irradiation time, etc.). Small discrepancies between experimental and calculated curves can be related to some destructive interference sources inside the materials (light reflected by the substrate, light scattered in the sample by defects, etc.).

ACKNOWLEDGEMENTS

This work was supported by the Ministry for Research and Culture of Saarland. The authors gratefully acknowledge the support of this work by Conselho Nacional de Pesquisa (P.W.O.) and Alexander Von Humboldt-Stiftung (P.J.). Our thanks are due to Drs. D. Hoebbel and T. Reinert for their help with the solid state NMR measurements.

REFERENCES

1. H. M. Smith, in *Principles of Holography*, 2nd edn., Wiley, New York, 1975.
2. J. Zhang, C. R. Carlen, S. Palmer and M. B. Sponsler, *J. Am. Chem. Soc.*, 1994, **116**, 7055.
3. G. Ozin, *Adv. Mater.*, 1992, **4**, 612.
4. S. Sakka and T. Yoko, in *Chemistry, Spectroscopy and Applications of Sol Gel Glasses*, Springer, Berlin, 1992, p. 89.
5. H. Schmidt, in *Chemistry, Spectroscopy and Applica tions of Sol Gel Glasses*, Springer, Berlin, 1992, p. 119.

6. (a) C. Sanchez and F. Ribot (eds.), *Proc. First Eur. Workshop on Hybrid Organic–Inorganic Materials*, Paris, 1993; (b) Special issue, *New J. Chem.*, 1994, **18**.
7. (a) H. K. Schmidt, *MRS Symp. Proc.*, 1990, **180**, 961; (b) P. Judeinstein and C. Sanchez, *J. Mater. Chem.*, 1996, **6**, 511.
8. L. C. Klein (ed.), *Sol–Gel Technology for Thin Films, Fibers, Preforms, Electronics and Specialty Shapes*, Noyes, 1988.
9. (a) P. Souchay, in *Ions Minéraux Condensés*, Masson, Paris, 1969; (b) M. T. Pope, in *Heteropoly and Isopolyoxometallates*, Springer, Berlin, 1983.
10. M. T. Pope and A. Müller, *Angew. Chem. Int. Edn. Engl.*, 1991, **30**, 34.
11. E. Papaconstantinou, *Chem. Soc. Rev.*, 1989, **18**, 1.
12. F. Devreux, J. P. Boilot, F. Chaput and A. Lecomte, *Phys. Rev. A*, 1990, **41**, 6901.
13. R. Kasemann and H. K. Schmidt, *MRS Symp. Proc.*, 1994, **346**, 915.
14. R. Nass, E. Arpac, W. Glaubitt and H. Schmidt, *J. Non-Cryst. Solids*, 1990, **121**, 370.
15. M. Fournier, R. Thouvenot and C. Rocchiccioli-Deltcheff, *J. Chem. Soc., Faraday Trans.*, 1991, **87**, 349.
16. M. T. Pope, in *Heteropoly Blues, NATO Summer School Proc.*, Oxford, 1979.
17. C. Sanchez, J. Livage, J. P. Launay and M. Fournier, *J. Am. Chem. Soc.*, 1983, **105**, 6817.
18. P. Judeinstein and H. Schmidt, *J. Sol–Gel Sci. Technol.*, 1994, **3**, 189.
19. H. Eichler, J. Günther and W. Pohl, in *Laser-Induced Dynamic Gratings*, Springer, Berlin, 1976, Chap. 4, pp. 94–122.
20. H. Huang, J. A. Gilbert and H. J. Caufild, *SPIE Proc.*, 1992, **1667**, 172.
21. Q. Huang and H. J. Caufild, *SPIE Proc.*, 1991, **1461**, 302.
22. D. H. Close, in H. J. Caufild (ed.), *Optically Recorded Holography, Optical Elements, Handbook of Optical Holography*, Academic, New York, 1979, pp. 460–464.
23. G. W. Stroke, in *An Introduction to Coherent Optics and Holography*, Academic, New York, 1969, p. 225.
24. G. A. Shafeev and M. Wautelet, *J. Appl. Phys.*, 1992, **71**, 1638.
25. H. Krug, P. W. Oliveira, F. Tiefensee and H. Schmidt, *SPIE Proc.*, 1992, **1758**, 556.
26. P. Judeinstein, P. W. Oliveira, H. Krug and H. Schmidt, *Chem. Phys. Lett.*, 1994, **220**, 35.